Theoretical Study of the Relations between Structure and Photophysical Properties of Model Oligofluorenes with Central Keto Defect

Vladimír Lukeš,*,† Roland Šolc,† Hans Lischka,*,‡ and Harald Friedrich Kauffmann§

Department of Chemical Physics, Slovak University of Technology, Radlinského 9, SK-812 37 Bratislava, Slovakia, Institute for Theoretical Chemistry, University of Vienna, Währingerstrasse 17, A-1090 Wien, Austria, and Institute of Physical Chemistry, University of Vienna, Währingerstrasse 42, A-1090 Vienna, Austria

Received: March 24, 2009; Revised Manuscript Received: October 19, 2009

A systematic study of fluorenone and model oligofluorenes (trimer, pentamer, and heptamer) with a central keto defect was performed at ab initio Hartree−Fock (HF), density functional theory (DFT), configuration interaction singles (CIS), and time-dependent density functional theory (TD-DFT) levels. The main aim of this work was the investigation of the direct influence of the central keto defect on the optimal geometry, torsional potentials, and photophysical properties. From the structural point of view, the optimal all-trans electronic ground state geometries of studied oligomers exhibit a uniform torsion of ca. 44−45° (HF) or 37−38° (DFT). The optical excitation leads to the planarization of the fluorenone and fluorene fragments in the central part of the molecule (∼34° for CIS and ∼29° for TD-DFT). The computed excitation and fluorescence energies show a good agreement with the experiment. These presented theoretical results can be useful in designing novel fluorene−fluorenone optical materials as well as understanding of excitation−relaxation phenomena which may occur in various time-dependent optical experiments.

1. Introduction

Π-conjugated poly(fluorenes) (PF) have received great attention because of their broad technological applications in organic light emitting devices (OLEDs).[1,2] As a result of their large energy gap, they can be used also as host materials for an internal color conversion, and their liquid-crystalline properties allow the realization of polarized light emission. Moreover, these compounds may serve as model systems enabling the understanding of the properties of soft organic and biological matter. As it was shown in many experimental investigations, almost every photochemical, photophysical, or spectroscopic process in these systems involve the dynamics of photoexcited states.[3,4] In this context, the theoretical predictions and interpretations of experiments may have immediate technological implications offering valuable insight into the nature and behavior of excitations in opto-electronic materials.

The incorporation of fluorenone chromophores leads to changes in the emission properties of the polymer.[5−9] The low-energy emission ("green") band is dominant in the emission spectra. The energetic position of the low-energy emission band at about 2.3 eV in alkyl-PFs is very similar to the low-energy emission band of the fluorenone building block in statistical dialkylfluorene/fluorenone copolymers.[10] The contribution of keto defect sites to the emission is more pronounced in electroluminescence when compared to photoluminescence. The reason behind this observation is the presence of two simultaneous processes that contribute to the low-energy emission: (1) energy transfer from the singlet excitons on the PF main chain to keto defect sites and (2) trapping of charge carriers at the fluorenone defect sites followed by subsequent emissive recombination events.[11] The second process is improbable in photoluminescence experiments and increases the contribution of the defect-site-related low-energy electroluminiscence band. To explain the experimental results of oligofluorenes or PFs, various quantum chemical studies were presented.[12−14] Theoretical works[15,16] taking fluorenone-containing oligomers into account indicated that the green emission can originate from the fluorenone moieties as a consequence of an efficient energy transfer to these sites and the localization of the excitons on the fluorenone units. Although these semiempirical calculations based on AM1 and ZINDO Hamiltonians provide a certain description of the lowest electronic $\pi-\pi^*$ states, a complex theoretical characterization of optimal geometries using modern quantum chemical methods, corresponding higher vertical electronic states, and their torsional dependencies is still absent for these molecular systems.

To gain deeper insight into the effect of keto group on the photophysical properties of PF, we will focus the quantum chemical calculations on fluorenone and model symmetric oligofluorenes (trimer, pentamer, and heptamer) with a central keto defect, see Figure 1. The optimal geometries of the electronic ground (GS) and lowest singlet and triplet excited (ES) states will be calculated using Hartree−Fock (HF),[17] density functional theory (DFT),[18] time-dependent density functional theory (TD-DFT),[19] and configuration interaction singles (CIS)[20] methods. On the basis of the obtained theoretical structures, the vertical excitations or de-excitations will be calculated and the structural relationships with these quantities will be analyzed. All computed quantities will be compared with available experimental data. Finally, a detailed insight into the electronic GS and lowest vertically singlet excited torsional potentials between fluorenone−fluorene fragments will be presented.

2. Quantum-Chemical Methods

The electronic ground state geometries of the fluorenone (**OF_1K**) and fluorene oligomers with a central keto defect

* To whom correspondence should be addressed. E-mail: vladimir.lukes@stuba.sk (V. L.), hans.lischka@univie.ac.at (H. L.).
† Slovak University of Technology.
‡ Institute for Theoretical Chemistry, University of Vienna.
§ Institute of Physical Chemistry, University of Vienna.

10.1021/jp902658u
Published on Web 11/23/2009

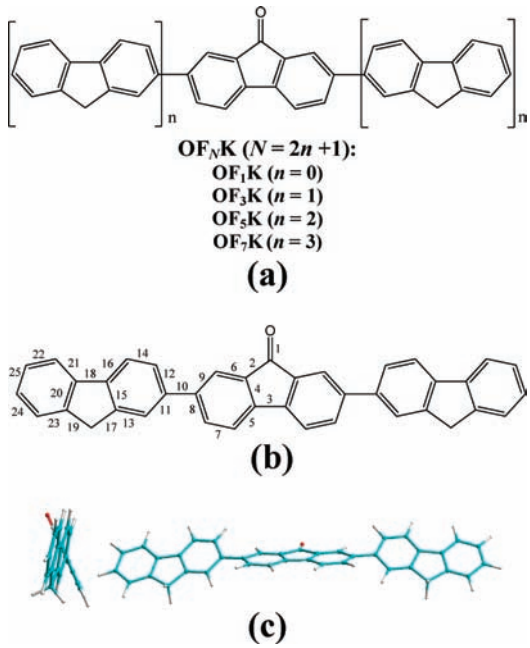

Figure 1. Structural schemes of investigated systems (a), bond numbering of **OF$_1$K** and **OF$_3$K** molecules (b), and front and side views on optimal B3LYP geometry for **OF$_3$K** (c).

containing three, five, and seven aromatic units (**OF$_3$K**, **OF$_5$K**, and **OF$_7$K**, see Figure 1) were optimized using HF and DFT methods with the B3LYP functional.[21] The 6-31G(d)[22] basis set was used. The geometry optimizations of the lowest singlet and triplet excited state were performed using CIS and TD-DFT approaches. Because of the large variability of the possible orientations of dihedral angles between aromatic units, only all-anti conformations were investigated (see the orientations of dihedral angles between bonds 7−8−9 for **OF$_3$K** in Figure 1). The geometry optimization was restricted to C_s symmetry, and the molecules were oriented in such a way that the torsional axis coincides with the z axis.

On the basis of the optimized geometries, vertical electronic singlet and triplet transitions were calculated using TD-B3LYP functional. Fluorescence transitions ($S_1 \rightarrow S_0$) were obtained as the vertical de-excitation at the optimized geometry of the energetically lowest excited state. To estimate the role of solvent−solute interaction in the real spectra, the single-point TD-DFT optical transitions were also computed within the conductor-like screening model (COSMO)[23] for toluene ($\varepsilon_r = 2.38$ and solvent radius of 2.82 Å), chloroform ($\varepsilon_r = 4.90$ and solvent radius of 2.48 Å), and acetonitrile ($\varepsilon_r = 36.64$ and solvent radius of 2.16 Å) solvents. All calculations were performed using Turbomole program package.[24]

3. Results and Discussion

3.1. Optimal Geometries. Because the investigated oligomers exhibit a large number of conformational minima stemming from the presence of ring torsion around the single bonds located between the chromophoric units, we restricted our study only to the symmetric helically twisted all-trans conformation. Analogously, as in the *para*-phenylene, thiophene, or *para*-vinylphenylene oligomers, this conformation does not show a symmetry-broken structure, and it exhibits effective π-conjugation in comparison with other possible conformations.[25−27] Our calculations showed that the optimal electronic GS geometries are not planar as can be seen in Figure 1c from the side and front views on the optimal B3LYP geometry for **OF$_3$K**. The HF/6-31G(d) ground state geometries show a torsional angle between fluorene and fluorenone fragments of ca. 44° (see bonds 9−10−12 for **OF$_3$K**). Similar values of dihedral angles (∼45°) are found between fluorene fragments in **OF$_5$K** and **OF$_7$K** molecules. The optimal B3LYP/6-31G(d) geometries possess a slightly more planar structure, and the above-mentioned angles are ca. 37° (between fluorene and fluorenone) and ca. 38° (between fluorene and fluorene). The latter values agree very well with the experimentally observed value of ca. 36° [28] for alkylsubstituted polyfluorenes. If going to the electronically lowest excited singlet state (S_1), the dihedral angles between the fluorenone and fluorene fragments are decreased while the remaining angles between fluorenes are practically not changed with respect to the electronic ground state structures. CIS/6-31G(d) dihedral angles in the central part (between fluorenone and fluorene) are ca. 34°. The corresponding TD-B3LYP/6-31G(d) value is 29°. The presented data agree with the semiempirical AM1/CEO calculations of Franco and Tretiak.[15] They also reported the changes of dihedral angles between fluorene and florenone units ranging from 41° to 31° upon the optical excitation. I would not call the transition to triplet optical, since spin forbidden. Geometry optimization in the lowest excited triplet state (T_1) leads to the next smallest planarization (ca. 1°−4°) of the angles between the fluorene and fluorenone units in comparison with the optimal S_1 geometries calculated using the TD-B3LYP or CIS methods.The comparison of the bond lengths between the nonhydrogen atoms is also quite interesting. The computed bond lengths for the representative fluorenone (**OF$_1$K**) and **OF$_3$K** molecules are depicted in Figure 2. The smallest bond length is found for the C═O bond (no. 1). On the other hand, the distances between the C(H_2) or C(0) atoms and the neighboring carbon atoms (see bonds 2, 3, 10, 17, and 19) are the longest ones. The addition of the fluorene chromophore leads to structural changes with respect to a single fluorenone molecule. For example, the B3LYP bonds 8 and 9 are longer by ca. 0.01 Å while bonds 4 and 6 are equally shorter by ca. 0.01 Å. The electronic singlet or triplet excitation of the studied oligomers influences the first 10 bonds. It leads to the formation of a partially quinoide-type structure. Our TD-B3LYP or CIS results shown in Figure 2 indicate that the bonds between the chromophores are shortened (see bond 10 for **OF$_3$K**) while the adjacent intraring bonds (see bonds 4 and 5) are elongated in comparison with the HF or B3LYP ground state geometries. The largest effects are found in the central part of the molecule. The apparent differences between the optimal geometries of S_1 and T_1 states are connected with the C═O and neighboring C−C bonds (see bond nos. 1 and 2). The above-mentioned structural relaxations of the investigated lowest excited states are identical for other oligomers in the region of the central fluorenone molecule and neighboring fluorene bonds 10 and 11.

3.2. Absorption and Fluorescence Transitions. Vertically excited states are also connected with a molecular structure. The first 12 vertical excitation energies calculated at TD-B3LYP//B3LYP and TD-B3LYP//HF levels are summarized in Table 1. The smallest fluorenone molecule (**OF$_1$K**) exhibits the highest excitation energies with very small oscillator strengths in comparison with the studied oligomers. The addition of fluorene chromophores to fluorenone leads to a bathochromic shift and to the occurrence of an additional two or three transition energies with significant oscillator strengths ($f > 0.4$, see the transitions indicated by asterisk). In all systems, the lowest vertically excited state has $1^1A''$ symmetry with relatively small oscillator strength. As reported by Zojer et al.[14] by

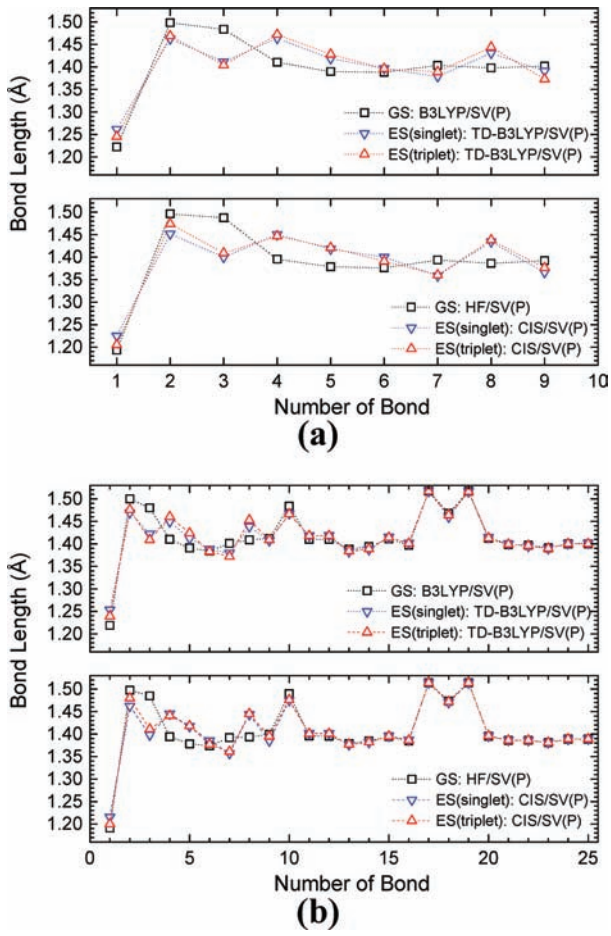

Figure 2. Calculated bond lengths for **OF_1K** (a) and **OF_3K** (b) molecules in the electronic ground and lowest excited singlet and triplet states.

semiempirical calculations, these transition from this electronic ground state S_0 to the S_1 state corresponds to an optically forbidden transition of n$-\pi^*$ character. The optical transitions corresponding to the higher states of A″ symmetry can have the larger oscillator strengths and can be classified as $\pi-\pi^*$ charge-transfer states. As indicated in Table 1, the transitions of A′ symmetry for small molecules are connected with negligible oscillator strengths. Only for the largest system **OF_7K** does the vertically excited state 4^1A′ have oscillator strength over 0.3.

To understand the global relationship between the structure and optical properties of studied **OF_3K**, **OF_5K**, and **OF_7K** oligomers, the electron absorption spectra bands were simulated. Einstein B coefficients were calculated from all TD-B3LYP excitation energies evaluated (up to the 20 transitions for **OF_7K**) and from relevant oscillator strengths on the basis of HF or B3LYP geometries. Next, the energy of every peak was modified by a Gaussian function with the height corresponding to the Einstein coefficient and with the width corresponding to an arbitrary phenomenological broadening constant (0.25 eV). The sum of all Gaussian functions plotted against the transition energy gives an approximation of the real spectrum. The computed bands show two or three main bands in the region ranging from 2.5 to 4.5 eV. The bands with the lowest energy have the smallest intensity in the investigated region. This band corresponds with the lowest energy and very broad experimental band. Our simulations based on the optimal HF as well as on the B3LYP geometries also indicate that the separation of the third peak depends on the oligomeric chain length. In the case of **OF_3K** molecule, the first peak is of a lower intensity than the second and third ones. For the largest **OF_7K** molecule, a very broad second band was obtained. All these findings are in agreement with the experimental spectrum (see Figure 3) measured in chloroform solution.[6]

According to the work of Zhan et al.,[29] a simple linear relationship between the two or three lowest theoretical (with significant oscillator strengths) and relevant experimental excitation energies can be derived. The depicted data exhibit the linear dependence as shown in Figure 4. The correlation coefficients

TABLE 1: Lowest 12 Calculated TD-B3LYP Vertical Excitation Energies E_{exc} (in eV) with Oscillator Strengths f (in Parentheses) for Optimal B3LYP and HF Geometries[a]

	TD-B3LYP//B3LYP/ 6-31G* $S_0 \rightarrow S_N$		TD-B3LYP//HF/ 6-31G* $S_0 \rightarrow S_N$	
molecule	symmetry	E_{exc} (f)	symmetry	E_{exc} (f)
OF_1K	1^1A″	3.11 (0.0033)*	1^1A″	3.27 (0.0032)*
	2^1A′	3.19 (0.0000)	2^1A′	3.32 (0.0000)
	2^1A″	4.04 (0.0263)*	2^1A″	4.17 (0.0215)*
	3^1A″	4.48 (0.0360)	3^1A″	4.61 (0.0321)
	3^1A′	5.00 (0.0000)	3^1A′	5.06 (0.0000)
	4^1A″	5.06 (0.8435)	4^1A″	5.17 (0.8485)
	5^1A″	5.10 (0.0514)	5^1A″	5.25 (0.0487)
	6^1A″	5.37 (0.1141)	6^1A″	5.49 (0.0080)
	7^1A″	5.58 (0.0001)	7^1A″	5.66 (0.0000)
	4^1A′	5.93 (0.0004)	4^1A″	5.99 (0.0005)
	8^1A″	6.02 (0.0001)	5^1A′	6.14 (0.0001)
	9^1A″	6.05 (0.1396)	9^1A″	6.17 (0.1329)
OF_3K	1^1A″	2.64 (0.2147)*	1^1A″	2.87 (0.1684)*
	2^1A″	3.12 (0.0001)	2^1A″	3.25 (0.0011)
	2^1A′	3.16 (0.0050)	2^1A′	3.35 (0.0046)
	3^1A″	3.57 (1.4790)*	3^1A″	3.77 (0.4170)
	4^1A″	3.65 (0.0001)	4^1A″	3.80 (0.9002)*
	3^1A′	4.00 (0.0022)	3^1A′	4.15 (0.0021)
	5^1A″	4.00 (0.0053)	5^1A″	4.15 (0.0056)
	4^1A′	4.04 (0.0019)	4^1A′	4.28 (0.9308)*
	6^1A″	4.13 (0.8980)*	6^1A″	4.37 (0.0079)
	5^1A′	4.22 (0.0017)	5^1A′	4.38 (0.0001)
	7^1A″	4.22 (0.0006)	5^1A′	4.40 (0.0094)
	6^1A′	4.41 (0.0098)	7^1A″	4.57 (0.0105)
OF_5K	1^1A″	2.55 (0.4853)*	1^1A″	2.81 (0.2983)*
	2^1A′	2.86 (0.0025)	2^1A″	3.09 (0.0029)
	2^1A″	3.12 (0.0016)	2^1A′	3.25 (0.0029)
	3^1A″	3.16 (0.0884)	3^1A″	3.36 (0.0027)
	4^1A″	3.33 (2.9460)*	4^1A″	3.60 (2.9048)*
	3^1A′	3.54 (0.0043)	3^1A′	3.71 (0.0023)
	4^1A′	3.59 (0.0198)	4^1A′	3.84 (0.0392)
	5^1A′	3.70 (0.0045)	5^1A″	3.92 (0.082)
	5^1A″	3.79 (0.9550)*	5^1A′	3.99 (0.0107)
	6^1A″	3.84 (0.1516)	6^1A″	4.05 (1.0167)*
	7^1A″	3.95 (0.0046)	7^1A″	4.16 (0.0247)
	8^1A″	3.99 (0.0036)	6^1A′	4.16 (0.0263)
OF_7K	1^1A″	2.54 (0.5279)*	1^1A″	2.79 (0.3599)*
	2^1A′	2.77 (0.0084)	2^1A′	3.02 (0.0056)
	2^1A″	2.95 (0.0028)	2^1A″	3.18 (0.0005)
	3^1A″	3.12 (0.0101)	3^1A″	3.25 (0.0043)
	3^1A′	3.20 (0.0020)	3^1A′	3.41 (0.0020)
	4^1A″	3.23 (4.5829)*	4^1A″	3.51 (4.4274)*
	4^1A′	3.38 (0.3225)	5^1A″	3.63 (0.0336)
	5^1A″	3.44 (0.0021)	4^1A′	3.65 (0.2969)
	5^1A′	3.56 (0.0190)	6^1A″	3.84 (0.6681)
	6^1A″	3.59 (0.6813)	5^1A′	3.85 (0.0351)
	7^1A″	3.71 (0.089)	6^1A′	3.90 (0.0011)
	6^1A′	3.73 (0.0044)	7^1A″	3.96 (0.1940)

[a] The asterisks indicate the energies which were correlated with relevant experimental data in Figure 4.

TABLE 2: Summary of the Dominant Optical Singlet Transitions for the Absorption ($S_0 \rightarrow S_N$) and Fluorescence ($S_1 \rightarrow S_0$) and Available Experimental Data[a]

	gas phase		toluene				chloroform				acetonitrile	
	$S_0 \rightarrow S_N$	$S_1 \rightarrow S_0$	$S_0 \rightarrow S_N$	exp.	$S_1 \rightarrow S_0$	exp.	$S_0 \rightarrow S_N$	exp.	$S_1 \rightarrow S_0$	exp.	$S_0 \rightarrow S_N$	$S_1 \rightarrow S_0$
OF_1K	3.10 (0.0033)	2.36 (0.0033)	3.02 (0.0027)		2.25 (0.0060)		2.97 (0.0024)	3.23	2.20 (0.0054)	2.42	2.91 (0.0020)	2.14 (0.0046)
	4.04 (0.0263)		4.00 (0.0360)				3.96 (0.0423)	4.04			3.91 (0.0507)	
OF_3K	2.64 (0.2141)	2.04 (0.2457)	2.59 (0.1918)		2.00 (0.2237)	2.33	2.55 (0.1787)	2.71	1.95 (0.2101)	2.12	2.51 (0.1621)	1.91 (0.1930)
	3.57 (1.4790)		3.56 (1.3576)	3.55			3.55 (0.7029)	3.54			3.55 (0.2204)	
			3.59 (0.1025)				3.57 (0.7433)				3.56 (1.2036)	
OF_5K	2.55 (0.4853)	2.02 (0.3836)	2.51 (0.4058)		1.97 (0.3448)	2.32	2.48 (0.3746)	2.71	1.93 (0.3214)	2.09	2.45 (0.3359)	1.90 (0.2922)
	3.33 (2.9460)		3.31 (3.0361)	3.40			3.31 (3.0621)	3.40			3.31 (3.1433)	
OF_7K	2.54 (0.5279)	2.00 (0.5258)	2.48 (0.4579)		1.96 (0.4718)	2.32	2.46 (0.4198)	2.71	1.92 (0.4391)	2.08	2.42 (0.3735)	1.88 (0.3986)
	3.23 (4.5829)		3.23 (4.6159)	3.34			3.23 (4.6759)	3.34			3.23 (4.7096)	

[a] All energies are in eV, and the values in parentheses stand for the oscillator strengths.

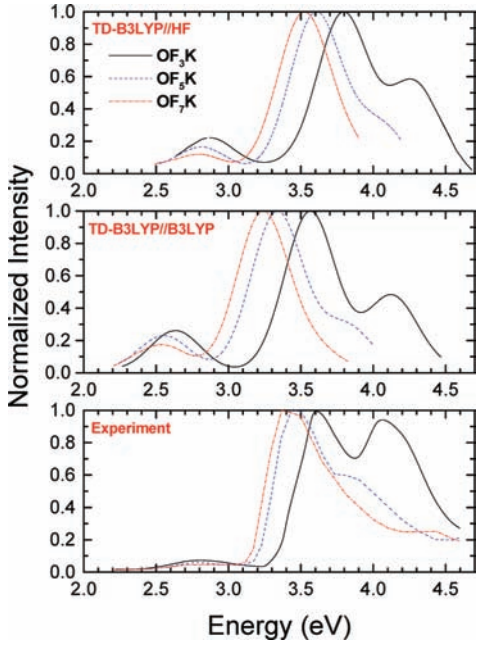

Figure 3. The simulated electron absorption bands of the investigated oligomers. The experimental data measured in $CHCl_3$ are taken from ref 6.

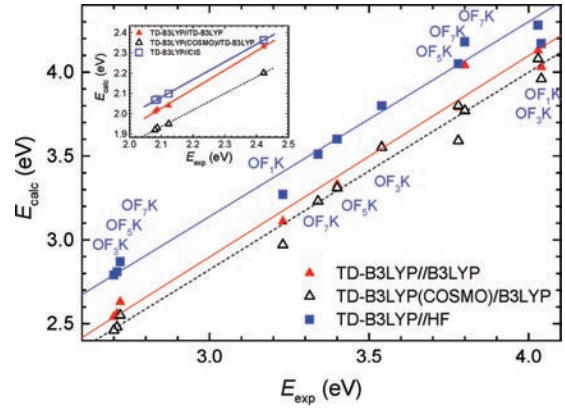

Figure 4. The correlation of selected dominant theoretical electronic excitation energies (see also Table 2) with the corresponding experimental values measured in $CHCl_3$. Inset: The correlation of theoretical fluorescence energies with experimental data measured in $CHCl_3$.[6] The COSMO calculations were performed for $CHCl_3$ solvent.

R for the dependence calculated excitation energies (E_{calc}) versus experimental energies (E_{exp}) is 0.992 for the B3LYP geometry and 0.994 for HF geometry.

$$E_{calc} = -0.70 + 1.20 \times E_{exp} \quad \text{TD-B3LYP//B3LYP} \tag{1}$$

$$E_{calc} = -0.35 + 1.16 \times E_{exp} \quad \text{TD-B3LYP//HF} \tag{2}$$

In both cases, the slopes are very similar. The values are negative, and for HF geometries, they are twice lower than that for the B3LYP ones. Although both theoretical results are shifted with respect to the experiment, the evaluated linear relationships can be used for the corrections of just-described systematic errors. Our TD-DFT calculations also showed that the oscillator strengths for the selected transitions are dependent on the molecular size (Table 1). The values for the $\pi-\pi^*$ transition increase linearly with increasing chain lengths from **OF1K** to **OF7K**. The increment is approximately 1.5 per 2 fluorenyl units. In contrast to the lowest energy $n-\pi^*$ transitions, the additive rule was not shown. This is in agreement with the experimental measurements[6] where the linear increase of molar extinction coefficients for $\pi-\pi^*$ transition was observed (e.g., in chloroform the $\varepsilon_{\pi-\pi^*}$ increase is approximately by 34 700 L mol^{-1} cm^1). The magnitude of $\varepsilon_{n-\pi^*}$ for $n-\pi^*$ transition is only chain-length dependent. On the other hand, the semiempirical calculations of Zojer et al.[14] predicted no dependence of the oscillator strength on the molecular size for $n-\pi^*$ transition. It seems that the TD-DFT method is able to offer a more realistic description of this behavior.

The TD-DFT lowest dipole-allowed excitation energies in the gas phase and in three representative dielectric media are collected in Table 2. The lowest singlet transitions are slightly red-shifted with increasing solvent polarity from toluene to acetonitrile. The highest sensitivity on the solvent polarity was found for fluorenone molecule (0.11 eV), and the lowest was found for **OF_7K** molecule (0.05 eV). The predicted positive solvatochromic response is in agreement with the experimental observations (see the experimental values for toluene and

chloroform in Table 2).[6] If we compare the gas-phase energies with the energies in toluene solvent, the differences are changed with the increase of molecular chain. The highest difference is for **OF_1K** (0.08 eV), and the lowest one is for **OF_7K** (0.03 eV). The minimal sensitivity on the environment is indicated for the second optical transition with dominant oscillator strength (see asterisk symbols in Table 1). The dependence of the calculated TD-B3LYP(COSMO) two or three lowest excitation energies on experimental energies in chloroform is also linear with the regression coefficient of 0. 9991 (see Figure 4).

$$E_{calc} = -0.71 + 1.18 \times E_{exp} \quad \text{TD-B3LYP(COSMO=CHCl}_3\text{)//B3LYP} \quad (3)$$

To understand the effect of the keto group on the absorption spectra for the lowest excitation energies with dominant oscillator strengths (see the transitions indicated by asterisk in Table 1), it is useful to examine the relevant (highest) occupied and lowest unoccupied molecular orbitals which play a dominant role in electronic transitions. These orbitals were evaluated for B3LYP geometries of **OF_1K** and **OF_5K** molecules (see Figure 5). As can be seen for the fluorenone (**OF_1K**) molecule, $1^1A''$, electron transition is excited from the highest occupied molecular orbital (HOMO) to the lowest unoccupied molecular orbital (LUMO). The HOMO orbital is delocalized over the carbon−carbon bonds which are perpendicularly oriented to the central bond 3. On the other hand, the LUMO orbital is delocalized over the oxygen atom and along bonds 2 and 3. In the case of the **OF_5K** oligomer, the HOMO to LUMO transition with 90% contribution dominates in the $1^1A''$ lowest excited state (see Figure 5b), too. However, the HOMO orbital is mostly delocalized in the central part as well as at the nearest neighboring fluorene units. The lobes of the LUMO orbital are practically delocalized over the central fluorenone unit. The next important transition comes from the HOMO to LUMO+1 orbital (see $4^1A''$ state in Table 1 and Figure 5b). In this case, the LUMO+1 orbital nicely shows the inter-ring bonding character, which is also reflected in the shortenings of the corresponding inter-ring C−C distances (see bond 10 in Figure 2 for HF and CIS results) in the relaxed lowest excited state as discussed in the previous section for **OF_3K** molecule. The electronic excitations for the last selected excited states ($5^1A''$ and $6^1A''$) are also connected with the transitions where the orbitals are delocalized over the fluorene units. It seems that the fluorenone chromophore may separate the photophysical processes on the oligomer chain for higher energies.

The first or second lowest excitation energies selected in Table 1 (see the values indicated by asterisk) uniformly decrease with the elongation of the chain. These data display good linear dependence (regression coefficients R are better than 0.998, see Table 4) on the inverse number of repeat units ($1/N$),

$$E_{exc} = A + \frac{B}{N} \quad (4)$$

The next possible evolution of the excitation energies with increasing chain length for larger oligomers may be achieved by using a model based on the Kuhn equation.[30] This function can be written as

$$E_{exc} = C\sqrt{1 + D\cos\frac{\pi}{N+1}} \quad (5)$$

The mutual comparison of the fitted parameters collected in Table 4 indicate that the theoretical polymer limits ($N \rightarrow \infty$) for the first lowest excited state estimated from eq 4 are 0.04 and 0.03 eV higher than the values obtained from eq 5; for example, for B3LYP geometries, we obtained 2.42 eV (eq 4) and 2.46 eV (eq 5). The predicted polymer limits of the relevant second selected excitation energies evaluated from eqs 4 and 5 exhibit higher differences of 0.08 and 0.09 eV. All these theoretical energies are systematically underestimated in absolute values by about 0.18−0.43 eV with respect to the experimental results. This systematic underestimation and the deficiencies of TD-DFT with increasing N are well-known. Similar findings for various aromatic molecules were published by Dierksen and Grimme.[31]

On the basis of the geometries optimized for the $1^1A''$ excited state, the fluorescence spectra were calculated. As seen in the inset of Figure 4, these values show again the linear correlation with experimental data (R is over 0.999).

$$E_{calc} = 0.05 + 0.94 \times E_{exp} \quad \text{TD-B3LYP//TD-B3LYP} \quad (6)$$

$$E_{calc} = 0.22 + 0.82 \times E_{exp} \quad \text{TD-B3LYP(COSMO=CHCl}_3\text{)//TD-B3LYP} \quad (7)$$

$$E_{calc} = 0.25 + 0.87 \times E_{exp} \quad \text{TD-B3LYP//CIS} \quad (8)$$

The theoretical fluorescence energies calculated for the gas phase or chloroform solution are not significantly underestimated in comparison with the experimental values as in the case of excitation energies (see Table 4). Therefore, the asymptotic theoretical data and the experimental values[6] measured in $CHCl_3$ agree satisfactorily. The theoretical values estimated from eqs 4 and 5 are practically identical with the experimental limits (2.01 and 2.03 eV). The estimated solvent effect originating from the keto defect is more significant for the solution of higher polarity. For example, the calculated fluorescence energy of **OF_3K** molecule shifts from 2.00 to 1.91 eV when going from toluene to acetonitrile. The higher sensitivity of the fluorescence spectra on solvent polarity was also observed experimentally for the real alkylsubstituted oligofluorenes as can be seen from the data for toluene and chloroform solvents in Table 2.

In Table 3, the energy difference between the S_0 ground state and the T_1 lowest triplet state calculated on the basis of optimal S_0 geometry is also shown. The evolution with chain length of the $S_0 \rightarrow T_1$ energy difference is slower than that of the $S_0 \rightarrow S_1$ excitation. The singlet−triplet energy difference is only lowered by ∼0.2 eV when going from the **PFO** to **PFO7**. The corresponding singlet−singlet absorption is characterized by a batochromic shift that amounts to ∼1.2 eV. The predicted energies exhibit the linear relations on the inverse number of repeat units N (see eq 4), or the Kuhn's equation (see eq 5) can be also used for the fitting of the dependence. The slope of the linear function is bigger (0.42 eV per unit) for the $S_0 \rightarrow S_1$ transition than that for $S_0 \rightarrow T_1$. The smaller gain for the length dependence of the transition to the triplet state as compared to the singlet state was experimentally observed for the oligofluorene series without keto defect. The observed slope for absorption is 1.23 eV per unit, whereas 0.89 eV per unit is connected with $S_0 \rightarrow T_1$ transition.

The shape of the experimental fluorescence spectra of investigated molecules exhibits for the low temperatures the vibronic splitting. For example, the splitting for **PFO3** or **PFO5** molecules at 77 K is about 160 meV. To estimate the origin of this vibronic structure, the additional calculation of the Huang−Rhys (HR) factors and mass-weighted displacements[32] was performed for **PFO** and **PFO3** molecules within the harmonic approximation of undistorted oscillators (see Tables 1S and 2S of the Supporting Information). The calculated nonzero HR factors for **PFO3** molecule belong to the A′

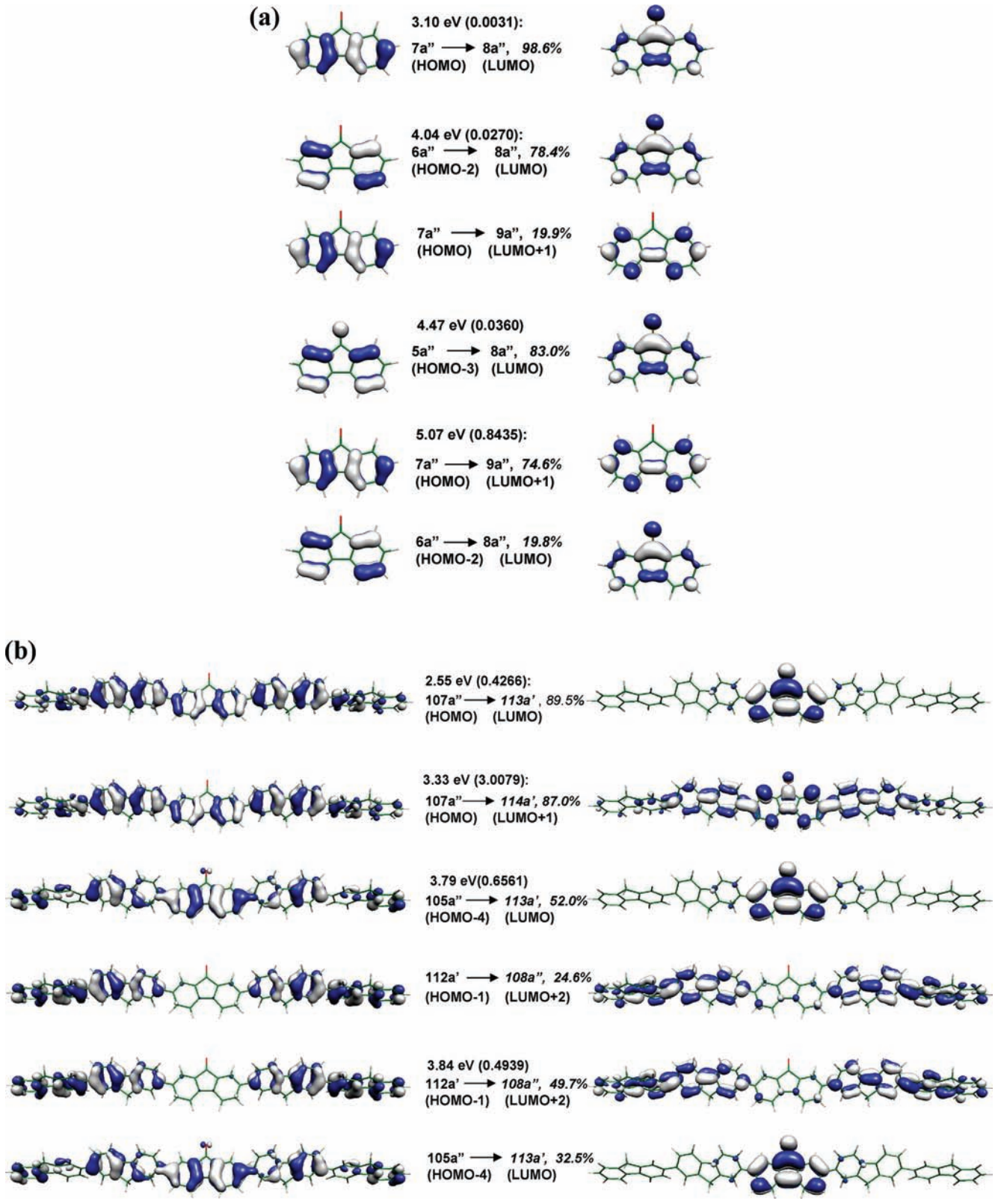

Figure 5. Plots of the B3LYP/6-31G(d) molecular orbitals significantly contributing to the selected lowest energy transitions of **OF_1K** ($1^1A''$) and **OF_5K** ($1^1A''$, $4^1A''$, $5^1A''$, and $6^1A''$) molecules. Values in parentheses represent oscillator strengths, and the values in italic stand for the percentages of the excitation contributions to individual transitions.

symmetry. The largest HR factors (higher than 0.01) corresponding to the frequency interval 1000−1800 cm^{-1} are connected with the out-of-plane CH and CC bending torsional vibrations and CC ring stretches (see Table 2S and Figure 1S of the Supporting Information). The C═O stretch vibration occurring in the central part of the molecule occurs in the all selected modes.

3.2. Ground State and Vertically Excited Torsional Potentials. Electronic ground state torsional potential between fluorenone and fluorene units was computed for the smallest

TABLE 3: Summary of the Lowest Vertical Triplet TD-B3LYP/6-31G* Transitions Calculated for the Optimal B3LYP/6-31G* Geometry[a]

	gas phase	toluene	chloroform	acetonitrile
	$S_0 \rightarrow T_1$	$S_0 \rightarrow T_1$	$S_0 \rightarrow T_1$	$S_0 \rightarrow T_1$
OF_1K	2.43	2.38	2.35	2.31
OF_3K	2.12	2.08	2.07	2.04
OF_5K	2.09	2.05	2.04	2.01
OF_7K	2.08	2.04	2.03	2.01

[a] All energies are in eV.

OF_3K oligomer by changing the torsional angles by 10° steps. The geometries were optimized for each setting of dihedral angles (see Figure 1). The computed electronic ground state B3LYP/6-31G(d) torsional potential with respect to the energy minimum is shown in Figure 6. The obtained curve exhibits two minima for nonplanar structures that correspond to the most stable conformations. These minima are separated by the barriers corresponding to the perpendicular and planar orientations. The vibrational frequencies of these specific geometries were also checked using vibrational analysis. The first-order saddle point (one imaginary frequency) for the perpendicular arrangement shows the highest energy barrier (0.126 eV = 2.91 kcal·mol^{-1}),

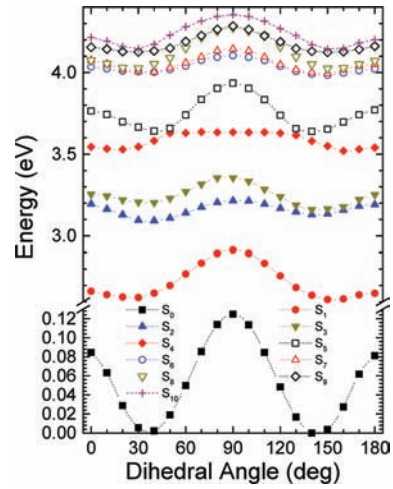

Figure 6. One-dimensional dependence of the electronic ground state (S_0) and verticaly excited states (S_1 to S_{10}) of **OF_3K** system on the torsion calculated at (TD-)B3LYP/6-31G(d) theoretical level. The ground-state energy minimum is taken as energy reference.

while the planar structures represent maxima with smaller energy barriers (0.085 eV = 1.96 kcal·mol^{-1}). In this context, a similar shape of electronic GS potential and barrier location were

TABLE 4: Fits of the Dependencies of Theoretical and Experimental Values for the Optical Transitions Selected in Tables 1 (See the Values Indicated by Asterisk) and 2 on the Number of Repeating Units *N*[a]

method	eq	parameters	*R*	method	eq	parameters	*R*
		TD-B3LYP//B3LYP				TD-B3LYP//TD-B3LYP	
$S_0 \rightarrow S_1$	4	$A = 2.42 \pm 0.01$	0.999	$S_1 \rightarrow S_0$	3	$A = 1.94 \pm 0.02$	0.996
		$B = 0.68 \pm 0.02$				$B = 0.39 \pm 0.03$	
		$(A = 2.36 \pm 0.01)$	(0.999)			$(A = 1.86 \pm 0.01)$	(0.994)
		$(B = 0.61 \pm 0.02)$				$(B = 0.34 \pm 0.03)$	
$S_0 \rightarrow S_N$*		$A = 2.89 \pm 0.03$	0.999		4	$C = 2.32 \pm 0.03$	0.989
		$B = 2.16 \pm 0.06$				$D = -0.29 \pm 0.03$	
$S_0 \rightarrow S_1$	5	$C = 3.10 \pm 0.02$	0.995			$(C = 2.19 \pm 0.02)$	(0.991)
		$D = -0.37 \pm 0.02$				$(D = -0.27 \pm 0.02)$	
$S_0 \rightarrow S_N$*		$(C = 2.96 \pm 0.02)$	(0.995)				
		$(D = -0.35 \pm 0.01)$					
		$C = 5.02 \pm 0.09$	0.991				
		$D = -0.65 \pm 0.03$					
		TD-B3LYP//B3LYP $S_0 \rightarrow T_1$					
	4	$A = 2.00 \pm 0.02$	0.995				
		$B = 0.42 \pm 0.03$					
		$(A = 1.96 \pm 0.01)$	(0.996)				
		$(B = 0.38 \pm 0.03)$					
$S_0 \rightarrow T_1$	5	$C = 2.42 \pm 0.02$	0.991				
		$D = -0.16 \pm 0.01$					
		$(C = 2.34 \pm 0.02)$	(0.993)				
		$(D = -0.15 \pm 0.01)$					
		TD-B3LYP//HF				TD-B3LYP//CIS	
$S_0 \rightarrow S_1$	4	$A = 2.69 \pm 0.01$	0.998	$S_1 \rightarrow S_0$	3	$A = 2.00 \pm 0.01$	0.994
		$B = 0.57 \pm 0.02$			4	$B = 0.36 \pm 0.03$	
		$A = 3.08 \pm 0.12$	0.989			$C = 2.35 \pm 0.02$	0.982
		$B = 2.08 \pm 0.22$				$D = -0.26 \pm 0.02$	
	5	$C = 3.26 \pm 0.02$	0.993				
		$D = -0.30 \pm 0.02$					
		$C = 5.14 \pm 0.16$	0.974				
		$D = -0.62 \pm 0.05$					
experiment[b]	4	$A = 2.57 \pm 0.04$	0.986	experiment[b]	3	$A = 2.01 \pm 0.01$	0.996
		$B = 0.64 \pm 0.08$				$B = 0.41 \pm 0.03$	
		$A = 3.31 \pm 0.05$	0.970		4	$C = 2.41 \pm 0.02$	0.986
		$B = 0.48 \pm 0.09$				$D = -0.29 \pm 0.02$	
	5	$C = 3.21 \pm 0.06$	0.961				
		$D = -0.34 \pm 0.04$					
		$C = 3.80 \pm 0.05$	0.951				
		$D = -0.23 \pm 0.03$					

[a] The parameters *A* and *B* of eq 4 and *C* of eq 5 are in eV. The symbol *R* denotes regression coefficient. The values in parentheses are obtained from the single-point TD-B3LYP(COSMO) calculations for chloroform. [b] Measured in chloroform, data taken from ref 6.

obtained for the torsion of simple phenylene rings around the connecting single bond. For example, B3LYP/SVP calculations[12] indicate the barrier height of 0.066 eV (1.53 kcal·mol^{-1}) for planar structure and of 0.103 eV (2.38 kcal·mol^{-1}) for the perpendicular one. Energy minimum was located at 37°. Qualitatively similar B3LYP results were reported by Fabiano and Della Sala.[33] They reported a minimum located at ca. 40° and barrier heights of 0.077 eV (1.78 kcal·mol^{-1}) for 0° and of 0.096 eV (2.12 kcal·mol^{-1}) for 90°. The best published ab initio estimates for the barriers extrapolated from the CCSD(T) energies using the continued fraction method of Goodson (CC-cf)[34] for the planar (perpendicular) barrier height are 0.083 eV = 1.91 kcal·mol^{-1} (0.086 eV = 1.98 kcal·mol^{-1}), while the values derived from experimental data[35,36] are 0.062 eV = 1.44 kcal·mol^{-1} (0.061 eV = 1.41 kcal·mol^{-1}) or 0.068 eV = 1.56 kcal·mol^{-1} (0.087 eV = 2.00 kcal·mol^{-1}). Although the performance of DFT method is known to show certain artifacts when dealing with energy barriers for internal rotation of aromatic systems,[37,38] the B3LYP data for biphenyl torsional potential curve do not differ significantly from the experimental potential within the upper limits of the error bars reported for these measurements (about 0.021 eV = 0.5 kcal·mol^{-1}).

The lowest 10 vertically excited-state potential energy curves ($S_0 \rightarrow S_1$) were calculated at the TD-B3LYP/6-31G(d) level on the basis of ground-state B3LYP optimized **OF$_3$K** geometries, and they are also shown in Figure 6. The depicted curves reflect the electronic GS potential with respect to the location of energy maxima and minima. Our calculations also indicate the separation of the lowest excited state (S_1) from the next states. On the other hand, the curves for S_3 and S_4 states exhibit the crossing at dihedral angles of 50° and 130°. The potential energy curves for the next higher excited states are quite closely spaced to each other and show mostly multiple intersections in the range of 20−80° and 100−160°. If we compare our results with simple oligophenylenes, the lowest excited state (e.g., 1^1B_1 for biphenyl) shows an energy minimum for a planar geometry and a maximum for the perpendicular one.[12] The next difference originates from the fact that this state crosses the next higher excited states (e.g., 1^1B_3 and 1^1B_1 curves at the dihedral angle of 44° for biphenyl).

4. Conclusions

We have performed a systematic theoretical study on the properties of excited states of fluorenone and three model fluorene oligomers with central keto defect. The optimized geometries were calculated for the electronic ground state ($1^1A'$) and lowest ($1^1A''$) excited states of each system. Our calculations showed that the electronic excitation leads to quinoide-type distortions and in particular to the shortening of the inter-ring bonds in the central part of a molecule and the bonds located in the vicinity of fluorenone units. The concomitant planarization of the central inner inter-ring torsions between fluorenone and fluorene fragments was also indicated.

The bands of absorption spectra were simulated using all the calculated excitation energies and oscillator strength. The obtained theoretical bands show two or three main bands in the region ranging from 2.8 to 3.8 eV. The intensity of the shoulder appearing at the lowest energies (long wavelengths) is minimally affected if the chain is elongated. Our simulations are in agreement with the experimental observation. Interesting conclusions can be made from the orbital analysis of the most significant electronic transitions. It was found that the keto defect located within the central fluorenone chromophore has distinct influence on the physical origin of electronic transitions. The lowest excitation energy for the **OF$_3$K** oligomer is based on the HOMO to LUMO transition. The HOMO orbital is mostly delocalized in the central part as well as at the nearest neighboring fluorene units. The lobes of LUMO orbital are practically delocalized over the central fluorenone unit. The electronic excitations for the higher electronic states are also connected with the transitions where the orbitals are not delocalized over the fluorenone units. Therefore, the role of central fluorenone chromophore for the symmetric model structure consists in the separation of photophysical processes on the side parts of oligomer chain. However, if the structural symmetry in the real situation will be broken, for example, because of the vibrational relaxation or environmental effects, this separation will be affected as well. Finally, the investigation of the electronic ground state torsional potential between fluorenone and fluorene units was performed for the **OF$_3$K** system. Our results showed that the lowest excited S_1 state seems to be well separated from the remaining ones with respect to torsional modes. The dependences for S_3 and S_4 states exhibit the crossing at dihedral angles of 40° and 145°. The potential energy curves for the next higher excited states are quite closely spaced to each other and show mostly multiple intersections in the range of 30−80° and 100−140°. On the basis of these predictions, the estimated role of torsional motion on the shape of spectra and spectroscopic shifts with respect to the mutual distortion of aromatic rings can help organic chemists tune optical properties of real oligofluorenes using alkyl substituents in the positions neighboring to the inter-ring bonds. All these above-mentioned features have their own importance in the possible application of studied oligofluorenes with keto defects in opto-electronic devices.

Supporting Information Available: The Cartesian coordinates and the total electronic energies of studied systems. Theoretical B3LYP/6-31G* vibrational spectrum, the projection of the mass-weighted geometry change between electronic states and Huang−Rhys factors for the optimal geometry of **PFO** and **PFO3** molecules. The visualization of the selected B3LYP/SV(P) normal modes for **PFO3** molecule with dominant Huang−Rhys factors. This material is available free of charge via the Internet at http://pubs.acs.org.

Acknowledgment. The authors acknowledge support by the Austrian Science Fund within the framework of the Special Research Program F16, Advanced Light Sources (ADLIS), Projects P18411-N19 and AF01618-NO2. The calculations were performed in part on the Schrödinger III cluster at the University of Vienna. R. Š. thanks also the Slovak Scientific Grant Agency (Projects No. VEGA 1/0774/08 and 1/0137/09) and the John von Neumann-Institut for the use of the supercomputer at the FZ Jülich.

References and Notes

(1) Brédas, J.-L.; Beljonne, D.; Coropceanu, V.; Cornil, J. *Chem. Rev.* **2004**, *104*, 4971.

(2) Barbieris, V. P.; Mikroyannidis, J. A. *Synth. Met.* **2006**, *156*, 1408.

(3) Milota, F.; Sperling, J.; Szöcs, V.; Tortschanoff, A.; Kauffmann, H. F. *J. Chem. Phys.* **2004**, *120*, 9870.

(4) Baldo, M. A.; Thompson, M. E.; Forest, S. R. *Nature* **2000**, *403*, 750.

(5) Gong, X.; Ostrowski, J. C.; Bazan, G. C.; Moscs, D.; Heeger, A. J.; Liu, M. S.; Jen, A. K.-Y. *Adv. Mater.* **2003**, *15*, 45.

(6) Chi, Ch.; Im, Ch.; Enkelmann, V.; Ziegler, A.; Lieser, G.; Wegner, G. *Chem.−Eur. J.* **2005**, *11*, 6833.

(7) Bliznyuk, V. N.; Carter, S. A.; Scott, J. C.; Klärner, G.; Miller, R. D.; Miller, D. C. *Macromolecules* **1999**, *32*, 361.

(8) Oelkrug, D.; Tompert, A. S.; Gierschner, J.; Egelhaaf, H.-J.; Hanack, M.; Hohloch, M.; Steinhuber, E. *J. Phys. Chem. B* **1998**, *102*, 1902.
(9) Nivsarkar, M. *Curr. Sci.* **1999**, *76*, 1391.
(10) Scandiucci de Freitas, P.; Scherf, U.; Collon, M.; Zojer, E.; List, E. J. W. *e-Polymers* **2002**, *0009*, 1.
(11) List, E. J. W.; Leising, G.; Schulte, N.; Schlütter, A. D.; Scherf, U.; Graupner, W. *Jpn. J. Appl. Phys., Part 2* **2000**, *39*, L760.
(12) Lukeš, V.; Aquino, A.; Lischka, H. *J. Phys. Chem. A* **2005**, *109*, 10232.
(13) Meeto, W.; Suramitr, S.; Vannarat, S.; Hannongbua, S. *Chem. Phys.* **2008**, *349*, 1.
(14) Zojer, E.; Pogantsch, A.; Hennebicq, E.; Beljonne, D.; Brédas, J. L.; de Freitas, P. S.; Scherf, U.; List, E. J. W. *J. Chem. Phys.* **2002**, *117*, 6794.
(15) Franco, I.; Tretiak, S. *J. Am. Chem. Soc.* **2004**, *126*, 12130.
(16) Pogantsch, A.; Heimel, G.; Zojer, E. *J. Chem. Phys.* **2002**, *117*, 5921.
(17) Roothan, C. C. J. *Rev. Mod. Phys.* **1951**, *23*, 69.
(18) Parr, R. G.; Yang, W. *Density-Functional Theory of Atoms and Molecules in Chemistry*; Springer-Verlag: New York, 1991.
(19) Stratmann, R. E.; Scuseria, G. E.; Frisch, M. J. *J. Chem. Phys.* **1998**, *109*, 8218.
(20) Foresman, J. B.; Head-Gordon, M.; Pople, J. A.; Frisch, M. J. *J. Phys. Chem.* **1992**, *96*, 135.
(21) Becke, A. D. *J. Chem. Phys.* **1996**, *104*, 1040.
(22) Gill, P. M. W.; Johnson, B. G.; Pople, J. A.; Frisch, M. J. *Chem. Phys. Lett.* **1992**, *197*, 499.
(23) Schäfer, A.; Klamt, A.; Sattel, D.; Lohrenzc, J. C. W.; Eckert, F. *Phys. Chem. Chem. Phys.* **2000**, *2*, 2187.
(24) Ahlrichs, R.; Bär, M.; Häser, M.; Horn, H.; Kölmel, C. *Chem. Phys. Lett.* **1989**, *162*, 165.
(25) Lukeš, V.; Aquino, A. J. A.; Lischka, H.; Kauffmann, H.-F. *J. Phys. Chem. B* **2007**, *111*, 7954.
(26) Liu, F.; Zuo, P.; Meng, L.; Zheng, S. J. *J. Mol. Struct.: THEOCHEM* **2005**, *726*, 161.
(27) Kwasniewski, S. P.; François, J. P.; Deleuze, S. M. *J. Phys. Chem. A* **2003**, *107*, 5168.
(28) Scherf, U.; List, E. J. W. *Adv. Mater.* **2001**, *14*, 477.
(29) Zhan, C. G.; Nichols, D. A.; Dixon, J. *J. Phys. Chem. A* **2003**, *107*, 4184.
(30) Kuhn, W. *Helv. Chim. Acta* **1948**, *31*, 1780.
(31) Dierksen, M.; Grimme, S. *J. Phys. Chem. A* **2004**, *108*, 10225.
(32) Gierschner, J.; Mack, H.-G.; Lüer, L.; Oelkrug, D. *J. Chem. Phys.* **2002**, *116*, 8596; see eqs 1 and 2.
(33) Fabiano, E.; Della Sala, F. *Chem. Phys. Lett.* **2006**, *418*, 496.
(34) Goodson, D. Z. *J. Chem. Phys.* **2002**, *116*, 6948.
(35) Bastiansen, O.; Samdal, S. *J. Mol. Struct.* **1985**, *128*, 115.
(36) Im, H.-S.; Bernstein, E. R. *J. Chem. Phys.* **1988**, *88*, 7337. This paper contains an error in eq 2, which calls for a correction according to. Beenken, W. J. D.; Lischka, H. *J. Chem. Phys.* **2005**, *123*, 144311.
(37) Karpfen, A.; Choi, C. H.; Kertesz, M. *J. Phys. Chem. A* **1997**, *101*, 7426.
(38) Sancho-García, J. C. *J. Chem. Phys.* **2006**, *124*, 124112.

JP902658U